

Conceptual design for the mid-infrared medium-resolution Echelle spectrometer (MIRMES) on SPICA Mission

Itsuki Sakon^{*a}, Yuji Ikeda^{b, c}, Naofumi Fujishiro^d, Hirokazu Kataza^e, Yoko Okada^f, Takashi Onaka^a

^aDepartment of Astronomy, Graduate Schools of Science, University of Tokyo,
7-3-1 Hongo, Bunkyo-ku, Tokyo 113-0033, Japan;

^bPhotocoding, 61-112 Iwakura-Kitakeda-cho, Sakyo-ku, Kyoto 606-0004, Japan;

^cDepartment of Physics, Faculty of Science, Kyoto-Sangyo University,
Motoyama, Kamigamo, Kita-Ku, Kyoto-City 603-8555, Japan;

^dCYBERNET SYSTEMS CO., LTD., Fujisoft Bldg., Kandaneibeicho,
Chiyoda-ku, Tokyo 101-0022, Japan;

^eInstitute of Space and Astronautical Science, Japan Aerospace Exploration Agency, 3-1-1
Yoshinodai, Chuo-ku, Sagami-hara, Kanagawa 252-5210, Japan;

^fUniversität zu Köln, I. Physikalisches Institut, Zulpicher Strasse 77, 50937 Köln, Germany

ABSTRACT

The Mid-Infrared Medium-Resolution Echelle Spectrometer (MIRMES) is one of the focal-plane instrument onboard SPICA mission proposed in the pre-project phase. It is designed for measuring the strengths and the profiles of lines and bands emitted from various phases of materials including ionized gas, gas-phase molecules, solid-phase molecules and dust particles in the wavelengths from 10 to 40 μ m. The MIRMES provides a medium resolution ($R=700$ – 1500) spectroscopic capability in the mid-infrared spectral range (10–36 μ m) with integrated field units of a field-of-view of about $12'' \times 6''$ for shorter wavelength range (10–20 μ m) and $12'' \times 12''.5$ for longer wavelength range (20–36 μ m). The science targets of the MIRMES and the results of the concept study on its optical design and the expected performance are described.

Keywords: infrared astronomy, infrared instrumentation, space mission, SPICA

1. INTRODUCTION

The core spectral range of SPICA resides between 20 and 200 μ m, in which SPICA will enable us to observe the sky faintest ever and the Holly Grail for SPICA waits to be discovered. In this spectral range, there exist a number of fine structure lines of ions and atoms, molecular lines, and band features stemming from solid particles together with the dust continuum emission, all of which provide significant and crucial information on the evolution of various phases of the interstellar medium (ISM) that can never be obtained at any other wavelengths. Many important optical and near-infrared line and band features of objects at high redshifts also come into this spectral range, which allow us for the first time to understand the physical condition of the remote universe that is hindered by strong absorption at shorter wavelengths. Whereas the SPICA far-infrared instrument (SAFARI; Swinyard et al. 2010) offers the most sensitive facility in the imaging and spectroscopic observations in the far-infrared and the mid-infrared camera w/wo lens (MIRACLE; Wada et al. 2010) provides the best imaging and low-resolution spectroscopy capability in the mid-infrared, a medium-resolution spectrograph in the mid-infrared (10–40 μ m) is an indispensable and key instrument to maximize the SPICA mission and carry out a large fraction of the primary scientific objectives discussed in the SPICA Mission Requirement Document (MRD). Here we propose the Mid-Infrared Medium-Resolution Spectrometer (MIRMES) as one of the focal-plane instruments onboard SPICA. The MIRMES will play a key role in the studies of interstellar and circumstellar physics and chemistry. In this proceedings, we summarize the science targets of the MIRMES and describe the results of the concept study on its optical design, and the expected performance.

*isakon@astron.s.u-tokyo.ac.jp; phone +81 3 5841-4276; fax +81 3 5841-7644

2. SCIENTIFIC TARGETS AND REQUIREMENTS ON INSTRUMENT SPECIFICATION

2.1 Scientific Targets

2.1.1 Physical Condition Diagnostics and Elemental Depletion in the ISM

The ISM consists of the various physical phases, between which the material circulation is crucial for the study of the evolution of galaxies (e.g., Tielens 2005) and the correct understanding of the physical conditions of each phase is indispensable. In the 10–40 μm wavelength range, there exist dozens of fine structure lines from ionized gas (e.g., [NeII] 12.81 μm , [Ne III] 15.56 μm , 36.01 μm , [NeV] 14.32 μm , [S III] 33.48 μm , 18.71 μm , [SIV] 10.51 μm , [PIII] 17.89 μm , [ArIII] 21.83 μm , [ArV] 13.07 μm , [OIV] 25.89 μm , [SiII] 34.82 μm , [Fe II] 25.99 μm , 35.35 μm , 17.94 μm , 24.5 μm , [FeIII] 22.93 μm , 33.04 μm). MIR fine-structure lines have advantages over optical lines for the unambiguous diagnostics of physical conditions of obscured regions because they are almost free from extinction and they are not very sensitive to the electron temperature in the ionized gas. The hardness of the interstellar radiation field (ISRF) can also be derived from a pair of transitions of the same element in different ionization stages, such as [NeII]15.56 μm / [NeII]12.81 μm (ionization potentials $\epsilon_{\text{ip}} \sim 41.0\text{eV}$ and 21.6eV , respectively), [SIV]10.51 μm / [SIII]18.71 μm ($\epsilon_{\text{ip}} \sim 34.8\text{eV}$ and 23.3eV), and [OIV]25.89 μm / [SiII]34.82 μm ($\epsilon_{\text{ip}} \sim 54.9\text{eV}$ and 8.2eV) (Thornley et al. 2000; Giveon et al. 2002; Hunt et al. 2010).

Molecular lines are important for the investigation of the warm ISM heated by UV photons or shocks. Rotational transitions of H₂ S(0) at 28.219 μm , H₂ S(1) at 17.035 μm , H₂ S(2) at 12.279 μm (critical density $n_{\text{cr}} < 10^3\text{cm}^{-3}$) are useful for the study of warm neutral phase of the ISM with temperatures ranging from ~ 100 and 1000K , in which these rotational transitions are an effective coolant (Hunt et al. 2010). Rotational transitions of ortho-H₂¹⁶O 7₂₅-6₁₆ at 29.836 μm and para-H₂¹⁶O 5₄₂-4₁₃ at 29.885 μm are good indicators for the presence of C-type shocks with a shock velocity of $> 10\text{km s}^{-1}$, since all gas-phase oxygen that is not bound in CO is rapidly converted into H₂O in warm ($\sim 300\text{K}$) molecular gas (Elitzur & de Jong 1978). Emission lines from lowest excited OH cross-ladder transitions at 28.94 μm ($v=0$, $^2\Pi_{1/2} \rightarrow ^2\Pi_{3/2}$, 7/2 \rightarrow 5/2) and at 34.62 μm ($v=0$, $^2\Pi_{1/2} \rightarrow ^2\Pi_{3/2}$, 7/2 \rightarrow 5/2) as well as highly excited OH pure rotational transitions of $v=0$, $J' \rightarrow J'-1$ ($J'=15/2$ to $69/2$) at wavelengths > 20 μm (e.g., $^2\Pi_{3/2}$ 19/2 \rightarrow 17/2 at 30.346 μm , $^2\Pi_{1/2}$ 17/2 \rightarrow 15/2 at 30.657 μm) are associated with the photo-dissociation of H₂O at $> 9\text{eV}$ and allow us to investigate the presence of hot dense gas (Hunt et al. 2010; Tappe et al. 2008).

Observations of [SiII] 34.82 μm , [FeII] 25.99 μm , [FeIII] 22.93 μm , [SIII] 33.46 μm [NII] 122 μm , [OI] 146 μm , and H α 12.4 μm enable us to determine the gas-phase abundance of Si and Fe, both of which are thought to be major constituents of interstellar grains, even in highly obscured regions. Since both Si and S are α -elements and, therefore, the elemental abundance ratio of Si/S is insensitive to the metallicity, the line ratios of [SiII]34.82 μm / [SIII]33.46 μm as well as [SiII]34.82 μm / [NII]122 μm can be used to derive the gas-phase abundance of Si in the ionized gas. Since Fe²⁺ and S²⁺ have similar ionization potentials, [FeIII] 22.93 μm / [SIII] 33.46 μm as well as [FeI]25.98 μm / [NII]122 μm are also good indicators for the gas-phase abundance of Fe in the ionized gas. A recent study of Spitzer observations of Galactic star-forming regions indicates that the abundance of silicon in the gas phase in the star-forming region is larger than that in cool interstellar clouds, suggesting the presence of Si-bearing dust species that is easily destroyed by the UV radiation other than silicates (Okada et al. 2008). A study of the elemental depletion, which is defined as the deficiency of a given element in the gas-phase compared to the reference abundance, provides us key information on the chemical link between the elements in the gas and solid phases in astrophysical environments. MIR and FIR imaging spectroscopy of the various lines with MIRMES and SAFARI will give us the first opportunity to investigate the depletion pattern among Si, Mg and Fe in the various phases of the ISM and give us a complete view of dust and gas chemistry in the ISM, which will be unable to be obtained by any other means (Okada et al. 2009).

2.1.2 Molecules in Circumstellar Disks and Stellar Atmosphere

Various molecular bands exist and have been identified in the 10–40 μm spectra in circumstellar disks of young sun-like stars (i.e., classical T Tauri stars) and in cool stars (i.e., brown dwarfs). In particular, search for pre-biotic molecules that contain C and N would be very interesting. Acetylene (C₂H₂) has the $\nu_5=1-0$ bending mode at 13.7 μm , cyanide (HCN) has the $\nu_2=1-0$ bending mode at 14.04 μm , ¹²CO₂ has the ν_2 bending mode at 14.9 μm , pure rotational lines of H₂O vapor lines reside in 12 μm and 40 μm , and rotational transitions of OH are observed in 20–31 μm . MIR bands of CO, N₂, H₂O, NH₃, and CH₄, have been observed in M, T, and T dwarfs. Weak NH₃ band features in 32–46 μm may appear in T dwarfs with $T_{\text{eff}} < 800\text{K}$ (Saumon et al. 2003). HCN is expected to be produced by the efficient photo-dissociation of N₂

in the disk atmosphere of sun-like stars and play a key role in the synthesis of pre-biotic molecules. Pascucci et al. (2009) have reported systematically higher line flux ratios of HCN/C₂H₂ in young sun-like stars (K1-M5) than in cool stars and brown dwarfs (M5-M9), suggesting the stronger UV-irradiation environment in sun-like stars. Further mid-infrared spectroscopic observations of molecules with SPICA/MIRMES will reveal the role of UV-photochemistry on the synthesis of organic molecules around low-mass young stars.

MIR spectroscopic observations of gas-phase molecules in the atmosphere of evolved low-mass stars will elucidate the chemical connection between the molecules and dust grains. The isotopic ratio of ¹³C/¹²C inferred from the H¹³CN (Q branch at 14.1 μm) and H¹²CN (2ν₂²-1ν₂¹ and 1ν₂¹-0ν₂⁰ bands at 14.00–14.04 μm) features is indicative of the second stage CNO cycling following the He burning in the very late thermal pulse (Herwig 2001; Evans et al. 2006) and thus useful to determine the evolutionary phase of the low-mass evolved star. Cyanides (H¹²CN and H¹³CN) and carbon chain molecules (polyynes), such as acetylene (C₂H₂ ν₅ Q branch at 13.7 μm), diacetylene (HC₄H ν₈ at 15.9 μm) and triacetylene (HC₆H ν₈ and ν₁₁ bands at 16.1 μm) have been detected in the post-asymptotic giant branch (AGB) star like V4334 Sgr (Sakurai's Object) (Evans et al. 2006). They are important building blocks for carbon dust grains and thus the detailed study of these species will be significant for the understanding of carbonaceous dust formation.

The warm molecular layer within a few stellar radii beyond, named as a MOLsphere (Tsuji 2000), has been detected in several red giants based on ISO spectroscopic observations, but no significant progress has been made since then because of the lack of efficient spectrometers with medium resolution in the MIR. The MOLsphere plays a key role in the mass-loss and the dust formation process. MIRMES will be the first sensitive spectrometer that can carry out a quantitative study the MOLsphere in detail after ISO/SWS and will provide crucial information on the chemical evolution of materials associated with the low-mass stellar activity.

2.1.3 Solid-phase Materials in Dense Interstellar Clouds

Comparison of the dust supply rate from stellar sources with the dust destruction rate in the ISM suggests that the supply from stars is not sufficient and interstellar grains must be formed in the ISM (Onaka 2000). In fact, a laboratory study indicates a possibility of silicate formation in cold environments (Nuth & Moore, 1988), but it is still quite uncertain what kind of dust will indeed form in dense clouds. Bradley (1994) and Bradley et al. (1999) suggest an interesting possibility that “glass with embedded metal sulfides (GEMS)” grains found in the interplanetary dust particles (IDPs) may be a good ISM dust analog. GEMS contains sulfur, which is not depleted in the diffuse ISM (Savage & Sembach, 1996). However, sulfur is largely depleted in dense clouds (Joseph et al., 1986), suggesting that dust formed in dense region may contain sulfur as GEMS. Keller et al. (2002) indicate that GEMS in IDPs have characteristic band features in the 20–30 μm region. MgS grains have a broad feature around 30 μm, whereas FeS grains show several band features in 20–50 μm. Broad features around 30 μm have been observed in a number of carbon stars, which are successfully accounted for by MgS grains (Hony et al., 2002). To our knowledge a similar broad 30 μm feature in the ISM has so far been detected only towards the Galactic center (Chan et al., 1997). The spectral region in 20–50 μm has not been explored with sensitive spectrometers and contains a number of interesting solid features untouched. The MIRMES together with the SAFARI are expected to reveal the dust species formed in the ISM with their high-sensitivity spectroscopy in mid- to far-infrared (Onaka et al. 2010).

2.1.4 Follow-up Spectroscopy of MIRACLE and SAFARI Objects

In addition to the scientific targets in our Galaxy and nearby galaxies mentioned above, the MIRMES is also expected to make a significant contribution in the follow-up observations of interesting objects that will have been discovered by the MIRACLE, SAFARI and JWST. In particular, the MIRMES will play a key role for the investigation of the physical nature of highly redshifted objects detected by the MIRACLE by using diagnostic lines in optical and/or NIR of the rest frame, depending on its redshift. The MIRMES spectroscopy is indispensable in maximizing the output of SPICA mission.

2.2 Requirements on Instrumental Specification

The SPICA/MIRMES is the medium resolution mid-infrared crossed echelle grating spectrometer with integral field units (IFU) and shall be designed so that the following instrument requirements are all fulfilled to accomplish the scientific targets in section 2.1.

The spectral range from 10 μm up to 36 μm shall be covered. The consistency in the absolute flux calibration and the observational simultaneity between shorter and longer wavelength spectra shall be achieved so that the ratios among fine structure lines and molecular hydrogen lines in 10–36 μm are accurately measured. To minimize the impact on the weight constraint and cover the wide spectral range, the MIRMES shall consist of short and long wavelength modules, which are designated as Arm-S and Arm-L, respectively, in the following. Simultaneous observations of the same sky area with the Arm-S and Arm-L are highly required to carry out mid-infrared spectroscopic observations of time-varying phenomena such as supernovae (SNe), luminous blue variables (LBVs), colliding-winds Wolf-Rayet binaries, novae, etc. For this purpose, a beam splitter shall be used at the entrance of the fore-optics to split the light from the object into the short and long wavelength parts and lead them to the Arm-S and Arm-L, respectively.

The width of the pseudo slit is optimized and set to λ_{max}/D , where λ_{max} is the longest wavelength for each module and D is the diameter of the primary mirror of the telescope. As for observations of extended sources, the difference in the slit width between the Arm-S and Arm-L will result in difficulties in deriving the true physical conditions. Therefore, the 2-D spectroscopy capability achieved by the IFU units in the fore-optics shall be required to ensure the consistency in the flux level between the two modules and construct continuous 10–36 μm spectral maps of extended sources accurately.

Among a number of lines from ions and molecules, several sets of the lines are located in narrow spectral ranges; For example, [OIV] 25.89 μm and [FeII] 25.99 μm lie at adjacent wavelengths with separation only by 0.098 μm , [FeII] 17.94 μm and [PIII] 17.885 μm lie even more closely with a separation only by $\Delta\lambda\sim 0.055\mu\text{m}$, H¹²CN at 14.04 μm and H¹³CN at 14.1 μm lie with a separation only by $\Delta\lambda\sim 0.06\mu\text{m}$ and ortho-H₂¹⁶O 7₂₅-6₁₆ at 29.836 μm and para-H₂¹⁶O 5₄₂-4₁₃ at 29.885 μm lie with a separation only by $\Delta\lambda\sim 0.05\mu\text{m}$. Decomposition of these lines shall be strongly required when employing them as diagnostic tools to infer the ISM conditions. Therefore, spectral resolution powers $R (= \lambda/\Delta\lambda) > 1000$ for Arm-S and $R > 600$ for Arm-L are required.

The efficient spectral mapping capability is required for the investigation of the properties of extended sources such as supernova remnants (SNRs) and ISM structures in nearby galaxies. The MIRMES shall be equipped with IFUs of the field of view of at least >5 arcsec and fields of view of >10 arcsec as a goal.

3. RESULTS OF THE CONCEPT STUDY AND THE EXPECTED PERFORMANCES

3.1 Overall Specifications of MIRMES

The present specifications of the SPICA/MIRMES based on the concept study are summarized in Table 1. The MIRMES consists of two channels; Arm-S, which covers from 10.0 μm to 19.9 μm with a moderately high spectral resolution power $R\sim 1490$ at 13 μm , and Arm-L, which covers from 19.5 μm to 36.1 μm with $R\sim 680$ at 27.8 μm . They share the same field of view (FOV) by means of a beam splitter at the entrance of the fore-optics. The Arm-S and Arm-L modules consist of reflective optics with echelle and cross-dispersing gratings. A Si:As detector array of 2048 \times 2048 pixels in size with a plate scale of 0.436 arcsec/pixel is used in the Arm-S module, while a Si:Sb detector array of 1024 \times 1024 pixels in size with a plate scale of 0.427 arcsec/pixel is used in the Arm-L module. The FOV of the MIRMES will be located adjacent to that of the MIRACLE. The aperture masks for Arm-S and Arm-L have sizes of 12'' \times 6'' and 12'' \times 12''.5, respectively. Each FOV area is split into 5 slitlets, each of which has a size of 12'' \times 1''.2 for Arm-S and 12'' \times 2''.5 for Arm-L, by means of the IFU units, respectively. The length of the pseudo slit is designed so that nearly an octave of a cross-dispersed echelle spectrum can fit onto the detector array without overlapping with different orders of the spectrum. The present specifications of MIRMES based on the concept study satisfy the instrumental requirements in section 2.2.

Table 1. Specification of the MIRMES

Parameters	Arm-S	Arm-L
detector array format	Si:As 2k×2k (pixels)	Si:Sb 1k×1k (pixels)
pixel pitch	25 (μm/pixel)	18 (μm/pixel)
pixel scale	0".403	0".485
wavelength coverage	10.0μm—20.0μm	19.5μm—36.1μm
spectral resolution ($R=\lambda/\Delta\lambda$)	1490 @13μm	680 @27.8μm
width of pseudo slit	1".2	2".5
length of pseudo slit	60"	60"
FOV size	12"×6".0	12"×12".5

In the Arm-S module, the incoming light is cross dispersed so that the spectrum over 4 different orders from $m=4^{\text{th}}$ to 7^{th} falls on the Si:As 2k×2k detector array. In the Arm-L module the incoming light is cross dispersed so that the spectrum over 4 different orders from $m=5^{\text{th}}$ to 8^{th} falls on the Si:Sb 1k×1k detector array. The wavelength range covered by the m^{th} order spectra is summarized in Table.2. λ_{min}^m and λ_{max}^m are defined by the wavelengths where the efficiency of the eschelle grating drops to 40% of the peak in the m^{th} order. The spectral formats of MIRMES Arm-S and Arm-L on the detector arrays are shown in Figure 1.

Table 2. Spectral formats of MIRMES Arm-S and Arm-L modules

Arm-S			Arm-L		
echelle order	$\lambda_{\text{min}}^m(\mu\text{m})$	$\lambda_{\text{max}}^m(\mu\text{m})$	echelle order	$\lambda_{\text{min}}^m(\mu\text{m})$	$\lambda_{\text{max}}^m(\mu\text{m})$
m=4	15.53	19.97	m=5	29.5	36.1
m=5	12.71	15.53	m=6	25.0	29.5
m=6	10.75	12.71	m=7	21.7	25.0
m=7	9.98	10.75	m=8	19.5	21.7

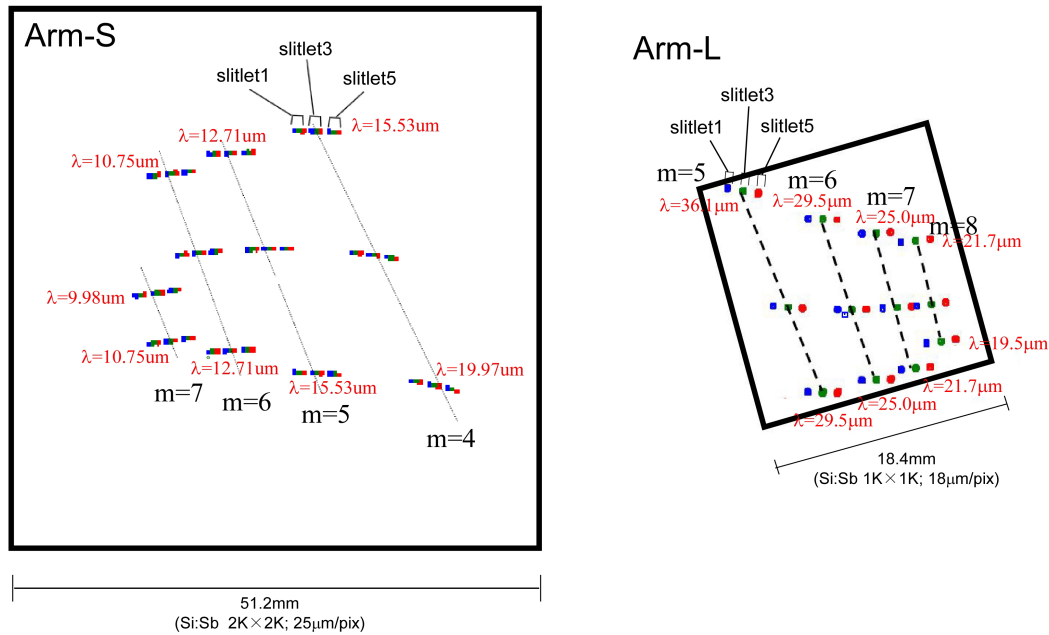


Figure 1. Spectral Formats of MIRMES Arm-S and Arm-L modules on the detector arrays

3.2 Optical Design of MIRMES

The MIRMES contains no moving parts. A blind mask for dark measurement is installed in the filter wheel placed at the entrance of the fore-optics and is shared with SPICA/MIRACLE. The FOV of MIRMES is located just next to that of MIRACLE on the focal plane. The light from the telescope is split by the beam splitter placed just after the first focal plane, and the shorter wavelength (10—20 μm) and longer wavelength (20—36 μm) light is introduced to the Arm-S and Arm-L modules, respectively. Each module consists of the fore-optics part including the IFU and the spectrograph.

3.2.1 Optical Design of the Image Slicer

Since the MIRMES Arm-S and Arm-L modules consist of all reflective elements, the “Content” type image slicer is adopted as the IFU for each of Arm-S and Arm-L. The specifications are summarized in Table 3. The incident $f/6$ beam from the focal plane of the telescope is converted into a $f/10$ beam by the F-conversion elliptic mirror and, then, is reflected by the concave field mirror. The reflected beam is refocused on the slicing mirrors through the Offner optics. Then the FOV is divided into 5 slitlets by the slicing mirrors and their pupil images are produced on the spherical pupil mirrors, which are placed independently on the output pupil positions of the Offner system. Finally, the slit images are refocused by the spherical mirror are aligned on the pseudo slit mirrors, forming in a pseudo slit image. Each pseudo slit mirror is tilted independently so that the central FOV ray of each slitlet becomes telecentric. The F-number of the output beam from the pseudo slit is $f/10$. The results of ray-tracing calculation of the IFU for MIRMES/Arm-S are shown in Figure 2.

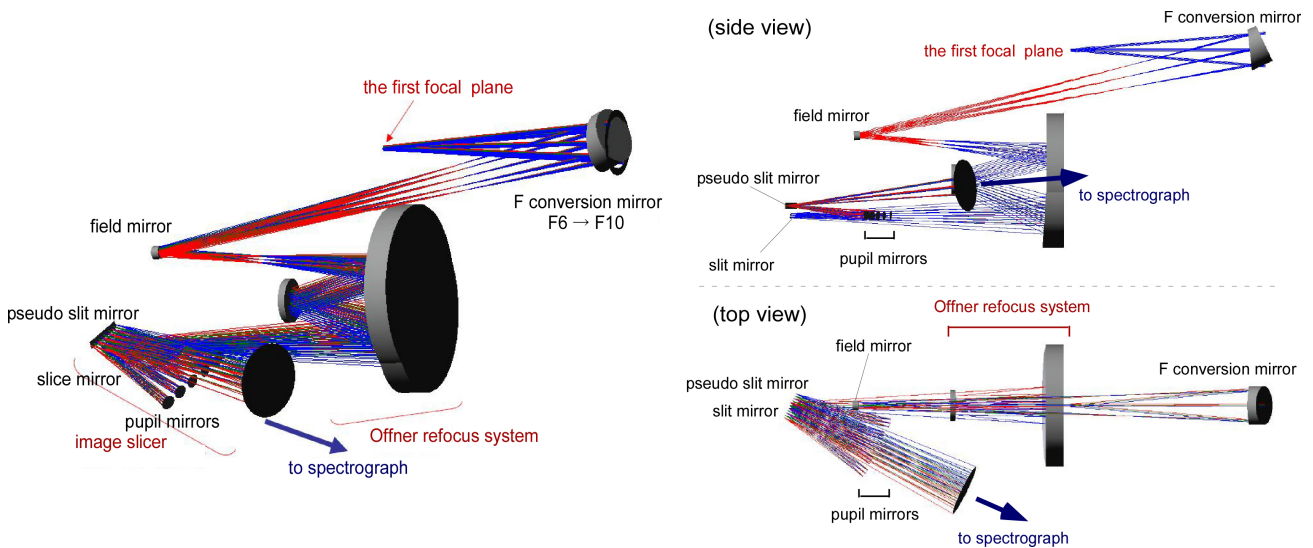


Figure 2. Results of ray-tracing calculation of the “Content” type image slicer for Arm-S

Table 3. Specification of the image slicer

Parameters	Arm-S	Arm-L
incident F-number	$f/6$	$f/6$
field-of-view	12” \times 6”	12” \times 12”.5
slice number	5	5
slice mirror width	250 μm	450 μm

3.2.2 Optical Design of Spectrograph for Arm-S

The collimator optics of the MIRMES/Arm-S consists of an off-axis non-spherical primary mirror and a free-form-surface secondary mirror. The effective focal length of the collimator system is 156.2mm and the pupil image with a size of 31.2mm in diameter is formed for the incident $f/10$ beam from the image slicer. The camera optics of the MIRMES/Arm-S consists of 3 free-form-surface mirrors. The final F-number of the camera system is $f/3.95$. The effective focal length of the camera system is 140.7mm. The cross disperser is placed just after the collimator system. The echelle grating is set after the cross disperser and splits incident $10\text{--}20\mu\text{m}$ light into 4 spectra of the echelle orders $m=4\text{--}7$. The optical path of the Arm-S spectrograph optics is shown in Figure 3.

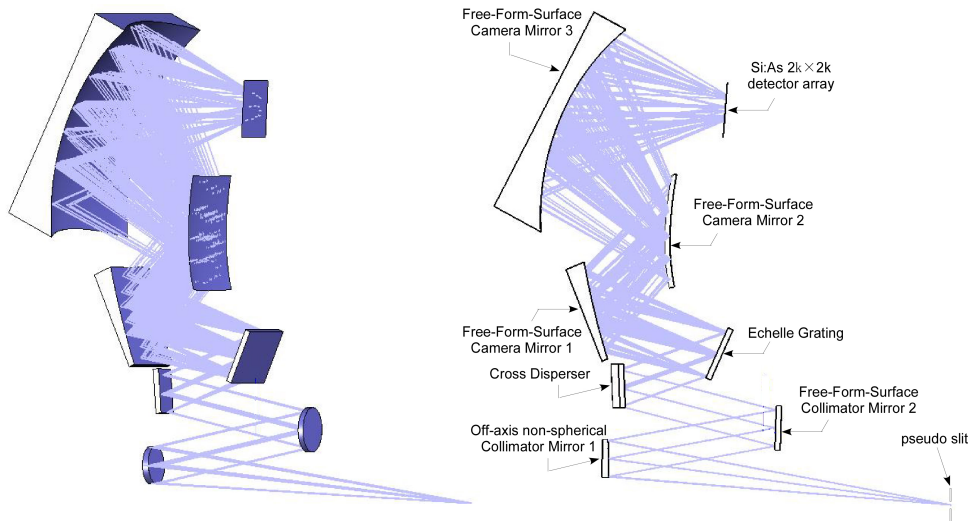


Figure 3. Ray-tracing results of spectrograph optics for Arm-S

3.2.3 Optical Design of Spectrograph for Arm-L

The collimator optics of MIRMES/Arm-L consists of an off-axis non-spherical primary mirror and a free-form-surface secondary mirror. The effective focal length of the collimator system is 156.2mm and the pupil image with a size of 31.2mm in diameter is formed for the incident $f/10$ beam from the image slicer. The camera optics of MIRMES/Arm-L consists of 3 free-form-surface mirrors. The final F-number of the camera system is $f/2.65$. The cross disperser is placed just after the collimator system. The echelle grating is set after the cross disperser and splits incident $20\text{--}36\mu\text{m}$ light into 4 spectra of the echelle orders $m=5\text{--}8$. The optical path of the Arm-L spectrograph optics is shown in Figure 4.

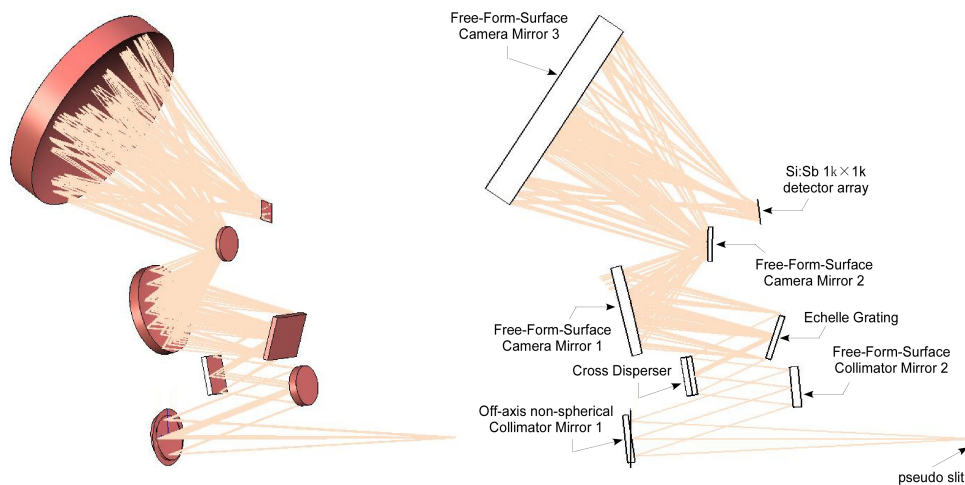


Figure 4. Ray-tracing results of spectrograph optics for Arm-L

3.3 Optical Elements

3.3.1 Cross Dispersers and Echelle Gratings

The parameters on grating pitch and blaze angle for cross dispersers and Echelle gratings for Arm-S and Arm-L are summarized in Table 4.

Table 4. Specification of cross dispersers and Echelle gratings

Dispersers	Parameters	Arm-S	Arm
Cross disperser	Grating pitch	45 μ m	92 μ m
	Blaze angle	~10deg	~9deg
Echelle grating	Grating pitch	87.3 μ m	195 μ m
	Blaze angle	~25deg	~29deg

3.3.2 Beam Splitter

A beam splitter is placed just after the focal plane of the telescope at the entrance of the fore-optics, by which the shorter wavelength light (10 μ m—20 μ m) is transmitted and the longer wavelength light (20 μ m—36 μ m) is reflected. The development of this element has been set forward aiming to fulfill the requirements that the reflectance in the 10—18 μ m be lower than 0.1% (with the 0.5% tolerance level) and that the reflectance in the 20—36 μ m be higher than 80% (with the 70% tolerance level).

3.3.3 Short Wavelength Cut-off Filter

A short-wavelength cut-off filter is installed before the beam splitter, by which only the light of wavelengths longer than 10 μ m is transmitted. The transmittance for the light of wavelengths shorter than 10 μ m should be less than 0.1% (with the 0.5% tolerance level) to avoid the effect of higher ($n \geq 2$) order light associated with the incident photons with $\lambda < 10\mu\text{m}$ on the Arm-S and Arm-L data.

3.3.4 Mirrors

Image slicer optics both for the Arm-S and Arm-L consist of 7 mirrors (a F conversion mirror, a field mirror, 2 mirrors for the Offner refocus optics, a slice mirror, pupil mirrors, and a pseudo slit mirror) and the spectrograph optics both for the Arm-S and Arm-L have 5 mirrors (a non-spherical mirror and a free-form-surface mirror for collimator system and 3 free-form-surface mirrors for the camera system). All of these mirrors are made of aluminum coated with Au and are required to have higher reflectance than 95% for any wavelengths in concern.

3.4 Volume and Structure

Each of the MIRMES/Arm-S and Arm-L modules fits within a box of 300[mm] \times 300[mm] \times 150[mm]. All the structural elements will be made of aluminum. The MIRMES optical elements are supported by the support rim of the instrumental optical bench (IOB), which is shared with MIRACLE and MIRHES to reduce the total weight (see Kataya et al. 2010; Wada et al. 2010). The total weight of the MIRMES optics is 4.4kg assuming all the optical elements are circular-shaped aluminum plate with a diameter as designed and a thickness corresponding to 20% of the diameter.

3.5 Thermal Design

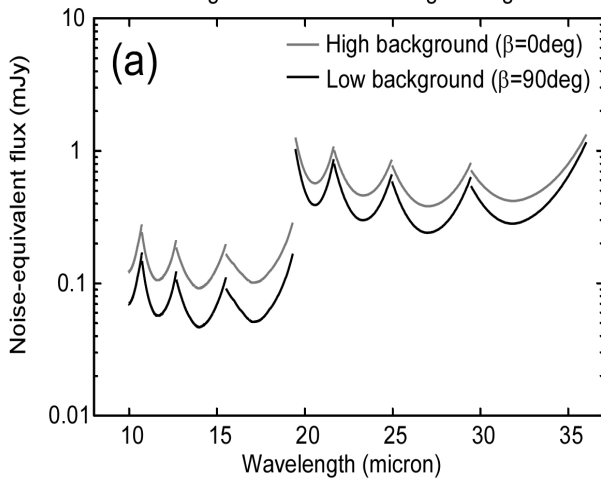
The SPICA/MIRMES contains no moving parts and will not have its own internal blind shatter for dark measurements nor the calibration lamp to monitor the response of detectors to reduce the weight. The MIRMES uses those functions by sharing the cold shatter and calibration lamp with the MIRACLE. The MIRMES will not make any impact on the thermal design concerning the moving parts. The thermal design associated with detector electronics of MIRMES is basically as the same as that of MIRACLE (see Wada et al. 2010)

4. EXPECTED PERFORMANCE OF MIRMES

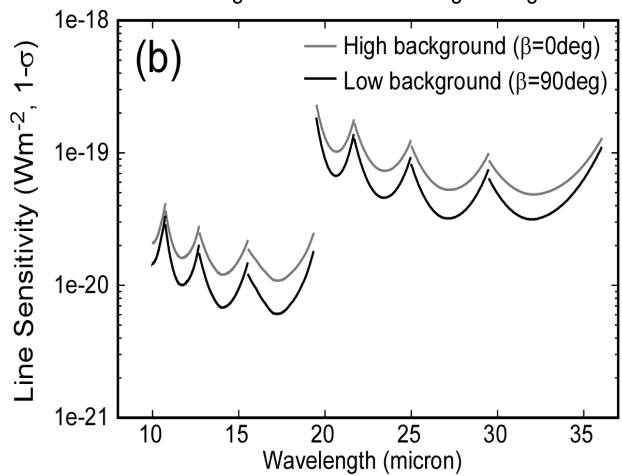
The expected MIRMES continuum sensitivities for point source, line sensitivity for point source and line sensitivity for extended source at low-and high-background for 600 sec ramp duration are shown in Figure 5(a), (b) and (c), respectively. The calculations have been made based on the assumption for readout noise of $n_{\text{readout}} = 5 e^-$ for Arm-S and $10 e^-$ for Arm-L and for detector dark current of $i_{\text{dark}} = 0.2 e^-/s$ for Arm-S and $0.5 e^-/s$.

MIRMES saturation limit for point source for the shortest ramp duration (2 sec) is shown in Figure 5(d). The results obtained for low-background case and high-background are indistinguishable at the scale of this plot. We assume that the linearity is guaranteed for less than half of the full well ($<0.5 \times 10^5 [e^-/\text{exposure}]$).

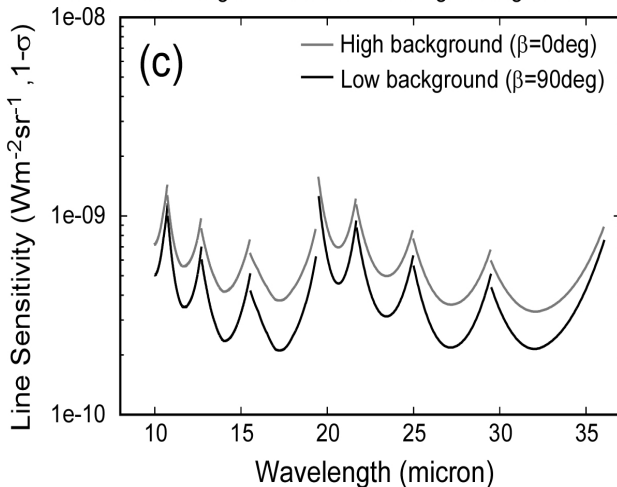
MIRMES Continuum Sensitivity for Point Source, 1-sigma
for 600 sec integration time at low & high background



MIRMES Line Sensitivity for Point Source, 1-sigma
for 600 sec integration time at low & high background



MIRMES Line Sensitivity for Extended Source, 1-sigma
for 600 sec integration time at low & high background



MIRMES Saturation Limit (1 exposure = 2[sec])

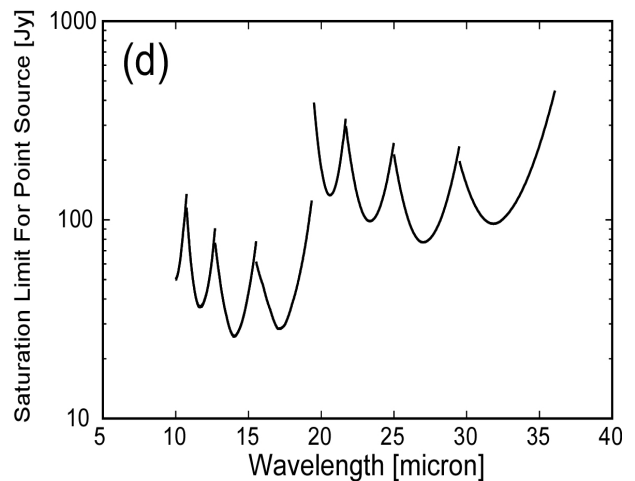


Figure 5. Expected sensitivity and saturation limit of MIRMES

5. SUMMARY

The Mid-Infrared Medium-Resolution Eschelle Spectrometer (MIRMES) is one of the focal-plane instrument onboard SPICA mission proposed in the pre-project phase. As a result of the concept study, the MIRMES is designed to have two channels; Arm-S, which covers from 10.0 μ m to 19.9 μ m with a moderately high spectral resolution power $R\sim 1490$ at 13 μ m, and Arm-L, which covers from 19.5 μ m to 36.1 μ m with $R\sim 680$ at 27.8 μ m. They share the same field of view by means of a beam splitter at the entrance of the fore-optics. The FOV of the MIRMES will be located adjacent to that of the the mid-infrared camera w/wo lens (MIRACLE). The aperture masks for Arm-S and Arm-L have sizes of 12" \times 6" and 12" \times 12".5, respectively. Each FOV area is split into 5 slitlets, each of which has a size of 12" \times 1".2 for Arm-S and 12" \times 2".5 for Arm-L, by means of the "content" type image slicer in the fore-optics part. The Arm-S and Arm-L spectrographs consist of all reflective optics with echelle and cross-dispersing gratings. A Si:As detector array of 2048 \times 2048 pixels in size with a plate scale of 0.436 arcsec/pixel is used in the Arm-S module, while a Si:Sb detector array of 1024 \times 1024 pixels in size with a plate scale of 0.427 arcsec/pixel is used in the Arm-L module. The present specifications of MIRMES based on the concept study satisfy the instrumental requirements given to accomplish the primary scientific objectives discussed in the SPICA Mission Requirement Document (MRD). The MIRMES will play a crucial role, particularly, in the studies of interstellar and circumstellar physics and chemistry and will be an indispensable and key instrument to maximize the SPICA mission.

ACKNOWLEDGEMENT

The authors thank SPICA MIRACLE team for taking charge of technical development of detectors and examinations on structural and thermal designs of MIRMES, which are generally common to those of MIRACLE. The authors also thank AKARI team members for useful discussion on sciences which are targeted by SPICA mission. The authors are grateful to the SPICA pre-project team members and the companies related to this program for their help and support.

REFERENCES

- [1] Bradley, J.P. "Chemically Anomalous, Preaccretionally Irradiated Grains in Interplanetary Dust From Comets", *Science*, 265, 925-929 (1994)
- [2] Bradley, J.P., Keller, L.P., Snow, T.P., et al., "An infrared spectral match between GEMS and interstellar grains," *Science*, 285, 1716-1718 (1999)
- [3] Chan, K.-W., Moseley, S. H., Casey, S., et al., "Dust Composition, Energetics, and Morphology of the Galactic Center", *The Astrophysical Journal*, 483, 798-810 (1997)
- [4] Elitzur, M. and de Jong, T., "A model for the maser sources associated with H II regions," *Astronomy and Astrophysics*, 67, 323-332 (1978)
- [5] Evans, A., Tyne, V.H., van Loon, J.Th., et al., "The Spitzer Infrared Spectrometer view of V4334 Sgr (Sakurai's Object)," *Mon. Not. of the Royal Astron. Soc.*, 372, 1227-1252 (2006)
- [6] Giveon, U., Sternberg, A., Lutz, D., et al., "The Excitation and Metallicity of Galactic H II Regions from Infrared Space Observatory SWS Observations of Mid-Infrared Fine-Structure Lines", *The Astrophysical Journal*, 566, 880-897 (2002) [Erratum: *ApJ*, 575, 585 (2002)]
- [7] Herwig, F., "The Evolutionary Timescale of Sakurai's Object: A Test of Convection Theory?", *The Astrophysical Journal*, 554, 71-72 (2001)
- [8] Hony, S., Waters, L. B. F. M., and Tielens, A. G. G. M., "The carrier of the 30 μ m emission feature in evolved stars. A simple model using magnesium sulfide," *Astronomy and Astrophysics*, 390, 533-553 (2002)
- [9] Hunt, L. K., Thuan, T. X.; Izotov, Y. I., Sauvage, M., "The Spitzer View of Low-Metallicity Star Formation. III. Fine-Structure Lines, Aromatic Features, and Molecules," *The Astrophysical Journal*, 712, 164-187 (2010)
- [10] Joseph, C. L., Snow, T. P., Jr., Seab, C. G., and Crutcher, R. M., "Interstellar abundances in dense, moderately reddened lines of sight. I - Observational evidence for density-dependent depletion," *The Astrophysical Journal*, 309, 771-782 (1986)
- [11] Kataza, H., Wada, T., Ikeda, Y., Fujishiro, N., Kobayashi, N. and Sakon, I., "Optical architecture of mid-infrared instrument (MIRACLE/MIRMES/MIRHES) on board SPICA," *Proc. of SPIE 7731*, in this volume (2010).

- [12] Keller, L. P., Hony, S., Bradley, J. P., et al., "Identification of iron sulphide grains in protoplanetary disks," *Nature*, 417, 148-150 (2002)
- [13] Nuth, J. A. and Moore, M.H., "SiH and the unidentified 4.6 micron feature," *The Astrophysical Journal*, 329, L113-L116 (1988)
- [14] Okada, Y., Onaka, T., Miyata, T., et al., "Si and Fe Depletion in Galactic Star-forming Regions Observed by the Spitzer Space Telescope", *The Astrophysical Journal*, 682, 416-433 (2008)
- [15] Okada, Y., Onaka, T., Kaneda, H. and Sakon, I., "Depletion Study of Si And Fe with Mid- and Far-Infrared Imaging Spectroscopy with SPICA," *Proc. of SPICA joint European/Japanese Workshop*, p.03008 (2009)
- [16] Onaka, T., "Evolution of Dust Grains in Galaxies and HII/L2", *ISAS Report, SP-14*, 83-90 (2000)
- [17] Onaka, T., Sakon, I., Kaneda, H. and Izumiura, H., "Evolving Gas and Dust in the Galaxy and galaxies to be seen by SPICA," *Proc. of SPICA joint European/Japanese Workshop*, p.03007 (2009)
- [18] Pascucci, I., Apai, D., Luhman, K., et al., "The Different Evolution of Gas and Dust in Disks around Sun-Like and Cool Stars," *The Astrophysical Journal*, 696, 143-159 (2009)
- [19] Saumon, D., Marley, M. S. and Lodders, K., "The Mid-Infrared Spectra of Brown Dwarfs", *ArXiv/astro-ph.10805* (2003)
- [20] Savage, B.D., and Sembach, K.R., "Interstellar Abundances from Absorption-Line Observations with the Hubble Space Telescope," *Annual Review of Astronomy and Astrophysics*, 34, 279-330 (1996)
- [21] Swinyard, B. M., "The safari far infrared imaging fourier transform spectrometer for the spica mission," *Proc. of SPIE*, 7731, in this volume (2010).
- [22] Tappe, A., Lada, C. J., Black, J. H. and Muench, A. A., "Discovery of Superthermal Hydroxyl (OH) in the HH 211 Outflow," *The Astrophysical Journal*, 680, L117-L120 (2008)
- [23] Tielens, A.G.G.M., "The Physics and Chemistry of the Interstellar Medium," Cambridge University Press, Cambridge, 1-510 (2005)
- [24] Thornley, M. D., Schreiber, N. M. F., Lutz, D., et al., "Massive Star Formation and Evolution in Starburst Galaxies: Mid-infrared Spectroscopy with the ISO Short Wavelength Spectrometer", *The Astrophysical Journal*, 539, 641-657 (2000)
- [25] Tsuji, T., "Water in Emission in the Infrared Space Observatory Spectrum of the Early M Supergiant Star μ Cephei," *The Astrophysical Journal*, 540, L99-L102 (2000)
- [26] Wada, T. and Katata, H., "Mid-infrared camera w/o lens (miracle) for SPICA," *Proc. of SPIE* 7731, in this volume (2010)